Deterioration evolution mechanism and damage constitutive model improvement of sandstone-coal composite samples under the effect of repeated immersion

Jiang, Tianqi
Department of Earth Resources Engineering, Kyushu University

Zhu, Chun
School of Earth Sciences and Engineering, Hohai University

Qiao, Yang
Oulu Mining School, University of Oulu

Sasaoka, Takashi
Department of Earth Resources Engineering, Kyushu University

他

出版情報：Physics of Fluids. 36 (5), pp.056611-1-056611-17, 2024-05-16. AIP Publishing
バージョン：

Physics of Fluids

RESEARCH ARTICLE | MAY 16 2024

Deterioration evolution mechanism and damage constitutive model improvement of sandstone–coal composite samples under the effect of repeated immersion

Tianqi Jiang (姜天琦) ; Chun Zhu (朱淳); Yang Qiao (乔洋) ; Takashi Sasaoka (笹岡孝司); Hideki Shimada (島田英樹); Akihiro Hamanaka (濱中晃弘) ; Wei Li (李卫) ; Bingbing Chen (陈兵兵)

Physics of Fluids 36, 056611 (2024)
https://doi.org/10.1063/5.0208619

Physics of Fluids ARTICLE pubs.aip.org/aip/pof

Deterioration evolution mechanism and damage constitutive model improvement of sandstone–coal composite samples under the effect of repeated immersion

Cite as: Phys. Fluids **36**, 056611 (2024); doi: 10.1063/5.0208619
Submitted: 15 March 2024 · Accepted: 1 May 2024 ·
Published Online: 16 May 2024

View Online Export Citation CrossMark

Tianqi Jiang (姜天琦),[1] Chun Zhu (朱淳),[2] Yang Qiao (乔洋),[3,4,a)] Takashi Sasaoka (笹岡孝司),[1] Hideki Shimada (島田英樹),[1] Akihiro Hamanaka (濱中晃弘),[1] Wei Li (李卫),[5] and Bingbing Chen (陈兵兵)[6]

AFFILIATIONS

[1]Department of Earth Resources Engineering, Kyushu University, Fukuoka 819-0395, Japan
[2]School of Earth Sciences and Engineering, Hohai University, Nanjing 210098, China
[3]Oulu Mining School, University of Oulu, Oulu, North Ostrobothnia FI-90014, Finland
[4]College of Civil Engineering, Tongji University, Shanghai 200092, China
[5]State Key Laboratory of Intelligent Construction and Healthy Operation and Maintenance of Deep Underground Engineering, China University of Mining and Technology, Xuzhou 221116, Jiangsu, China
[6]Zienkiewicz Institute for Modelling, Data and AI, Faculty of Science and Engineering, Swansea University, Swansea SA1 8EN, United Kingdom

[a)]**Author to whom correspondence should be addressed:** yang.qiao@oulu.fi

ABSTRACT

Underground reservoirs in coal mines, consisting of goafs (By goaf, we mean the space that remains underground after the extraction of valuable minerals), are commonly utilized for mine water storage and drainage, with their primary load-bearing structures being the "roof–coal pillar" systems. Consequently, this structure must endure the repeated immersion behavior resulting from fluctuations in the mine water level, resulting in the risk of geological disasters. This paper analyzes the variation in mechanical properties of sandstone–coal composite samples after repeated immersion cycles through axial loading tests. The results indicate that the water content of the sample exhibits a notable and rapid increase with each successive immersion cycle. This corresponds to a decrease in the stress threshold and modulus parameters of the samples. Moreover, the acoustic emission signals serve as indicators of the softening characteristics of the samples. With the increase in immersion cycles, there is an augmentation in both the frequency and extent of shear cracks. The non-linear failure characteristics of the samples become more pronounced. Consequently, water significantly weakens the cementing material between rock grains. Both sandstone and coal display a decrease in deformation resistance capabilities at a macroscopic level. The constitutive model of the composite sample was improved based on the degradation characteristics of mechanical strength and strain energy parameters, which offers enhanced accuracy in analyzing the degradation process caused by water immersion. This paper offers a crucial theoretical foundation for comprehending the deterioration evolution characteristics of the "roof–coal pillar" bearing structure affected by repeated immersion.

I. INTRODUCTION

Coal, as a fossil fuel, continues to maintain a prominent role in the energy consumption of numerous countries worldwide.[1,2] Presently, China has directed its coal mining focus toward the Western regions. However, this region faces challenges related to the uncoordinated and conflicting extraction of coal and water resources.[3] To solve this issue, scholars have proposed the concept of "underground reservoirs in coal mines," as depicted in Fig. 1.

Dams are frequently subjected to prolonged and repeated water immersion, which can pose a significant threat to the safe operation of reservoirs.[4] Therefore, numerous studies have been conducted by scholars to investigate various physical parameters of rocks during

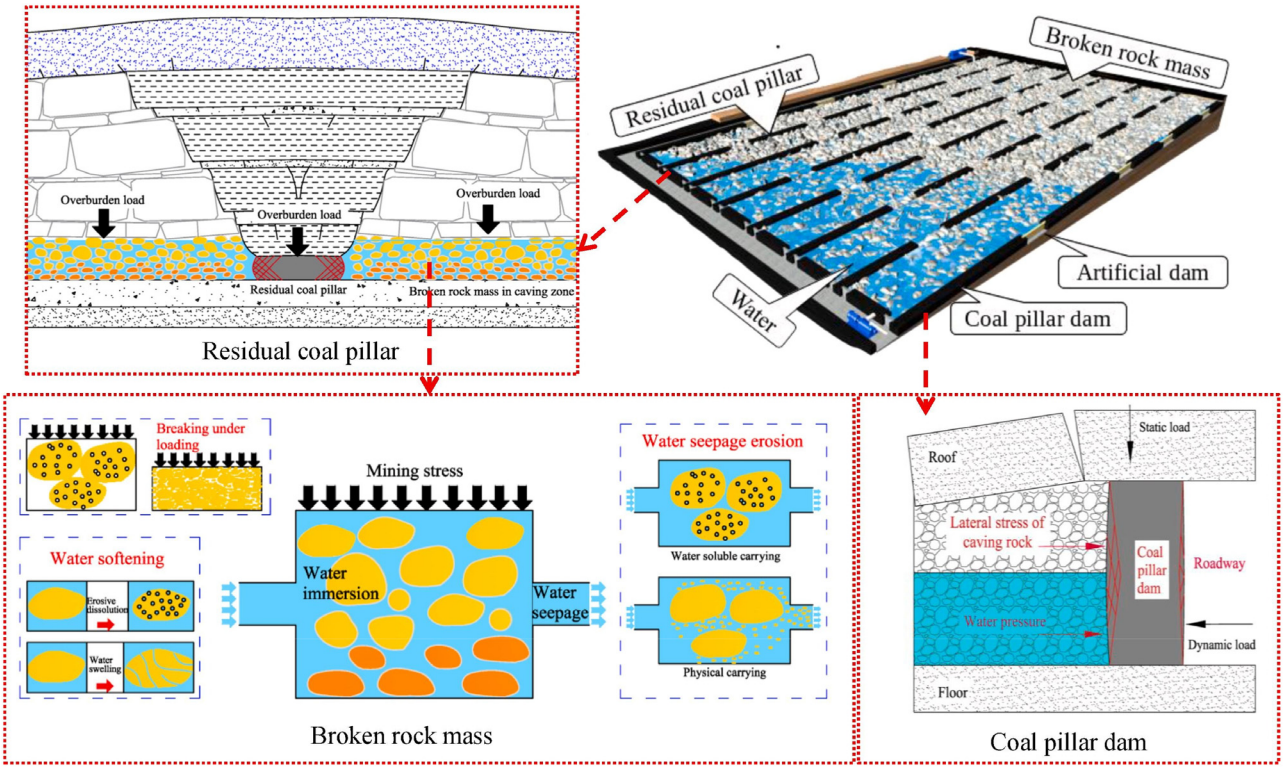

FIG. 1. Water–rock (coal) interactions in an underground reservoir. Zhang *et al.*, Tunnel. Underground Space Technol. **107**, 103657 (2021). Copyright 2023 Elsevier.[4]

water–rock interaction.[5] These parameters include changes in mass,[6] water content,[5] composition,[5] as well as the longitudinal wave velocity.[7] Additionally, mechanical properties like uniaxial compressive strength,[8] tensile strength,[9,10] triaxial compressive strength,[11] and elastic modulus[12,13] have also been tested. Scholars have also conducted various microscopic analyses to investigate the impact of water–rock interaction.[14–18] These studies have revealed that water–rock interaction weakens the mechanical strength of rocks.

Nevertheless, the dam structure of underground reservoirs in coal mines significantly differs from that of surface reservoirs. The main components of the dam structure in underground reservoirs consist of roof, floor, safety coal pillars, and artificial concrete pillars.[19] Furthermore, soft rocks, such as mudstone and coal,[19–21] exhibit higher sensitivity to water–rock interaction, including water absorption, softening, disintegration, expansibility, and seepage, compared to hard rocks.[22–26] Consequently, the long-term water–rock interaction of underground reservoirs in coal mines is more complex and obvious.[4] It is important to highlight that the coal mass and rock mass, which constitute the underground reservoir in coal mines, are not separate exist in goaf. Rather, they intricately intertwine and interlayer to create a roof–coal pillar composite structure.[27–29] This composite structure can be considered as a composite rock mass with distinctive properties.[29] Based on this understanding, numerous scholars have studied the influence of various factors, including lithology,[30] height ratio,[31] interface inclination angle,[32] cementation,[33] and moisture content,[34] on the mechanical strength of the rock-coal composite. However, the studies on roof–coal pillar composite structure under water–rock effects is limited, so it is necessary to further study the damage mechanism of rock–coal composite samples under repeated immersion.

In this study, axial loading tests were conducted on the rock–coal composite samples subjected to varying cycle numbers of repeated immersion. The aim was to investigate the impact of repeated immersion effect on the mechanical characteristic of the composite samples, thereby exploring the damage effects caused by the immersion process. The research findings presented in this paper will serve as a theoretical foundation for several practical applications. These include the design of waterproof coal pillars in deep coal mines, ensuring the safe operation of underground reservoirs in coal mines, and exploring the reuse possibilities of pumped storage power generation in the underground spaces of coal mines.

II. SAMPLE PREPARATION AND TEST SCHEME

A. Sample preparation

To ensure uniformity in both the environmental conditions and the mechanical characteristics of coal and sandstone, materials were sourced from the same coal seam and roof for this experiment. To minimize variability among samples, three identical test groups were established. Coal and sandstone blocks were then fashioned into samples with a diameter and height of 50 mm, adhering to standards outlined by the International Society for Rock Mechanics (ISRM) .[30] Following repeated immersion treatment, corresponding coal and sandstone samples were combined to form standard rock–coal composite samples, each with a diameter of 50 mm and a height of

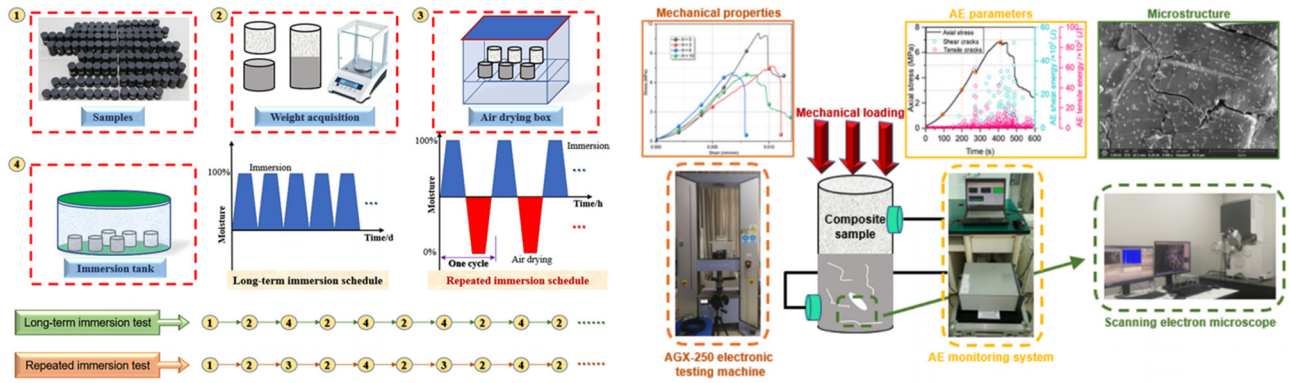

(a) Immersion test design

(b) Macroscopic mechanical tests and microscopic structural characterization

FIG. 2. Flow chart of repeated immersion and mechanical tests.

100 mm. It is important to note that during the assembly process, coal and sandstone were not bonded together. This is in order not to affect the water–rock interaction between the coal and rock interface.

B. Test scheme and equipment

The flow chart in Fig. 2 outlines the procedure for the long-term immersion test, as described in prior studies.[35,36] For the repeated immersion test in this manuscript, the design procedure was adapted from the long-term immersion test. Initially, samples were weighed after natural air drying. They were then fully immersed in a water immersion device for 24 h before being weighed again upon removal. Subsequently, the samples were air-dried in a closed air-conditioned room at 25 °C for 48 h until completely dry. This completed one cycle of the repeated immersion test, totaling 72 h. In this study, samples underwent 0–10 (N = 0–10) repeated immersion treatments to replicate dynamic changes in mine water levels within underground reservoirs.

Following the repeated water immersion test, physical and mechanical parameters of both sandstone and coal samples were assessed, as depicted in Fig. 2. Initially, scanning electron microscope tests (Nova Nano SEM450) were conducted on sandstone and coal samples subjected to repeated immersion cycles to evaluate damage to their skeletal structures. Subsequently, mechanical loading tests were carried out on the sandstone and coal samples under various repeated immersion cycles to gauge the deterioration of their mechanical strength. The testing setup for loading and monitoring primarily involved the Shimadzu AG-X250 electronic universal testing machine and the MISTRAS series PCI-2 acoustic emission (AE) system. The test employed displacement loading control, with a loading rate of 0.005 mm/s and a sensitivity set to 1%.

III. RESULTS AND ANALYSIS

A. Water content

The water content change in coal and sandstone directly indicates the extent of water accumulation within the internal defects, thereby indirectly reflecting the level of damage to the internal structure of the samples.[37] The water content of coal, sandstone, and their combination samples was determined by weighing the samples with different repeated immersion numbers. The results are shown in Fig. 3, in which the water content of individual sandstone samples increased from 0.227% to 0.267% with an increase in repeated immersion numbers. Similarly, the water content of individual coal samples increased from 3.169% to 5.513% over the same period. The water content of the individual sandstone samples showed a slight increase with the cycle number of repeated immersion tests increasing, but the increase was not significant. In contrast, the water content of the individual coal samples exhibited a significant increase, following a pattern of initially slow growth, followed by accelerated growth.

In addition, in on-site engineering fields, the coal–rock system consists of various rock (coal) seams that are interlayered, resulting in the formation of a unique rock–coal structure.[28] Upon this understanding, the sandstone–coal composite sample is treated as an intact rock sample to investigate its water content. The moisture content of the sandstone–coal composite sample increased from the initial value

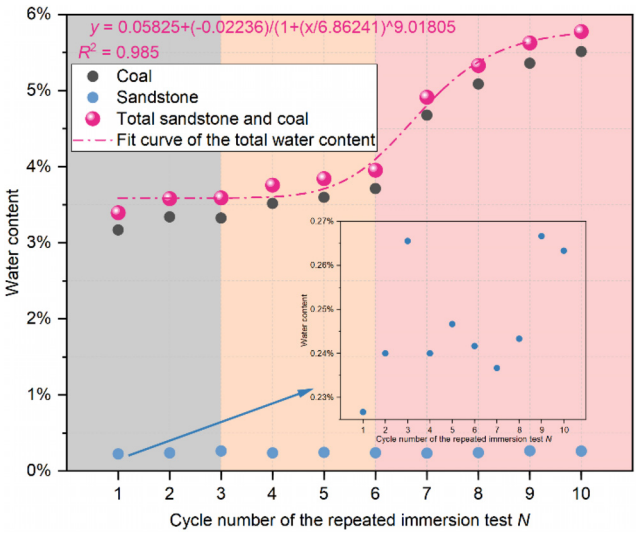

FIG. 3. Water content of samples under repeated immersion effect.

of 3.40% to 5.78%. Notably, the moisture content of the composite samples was found to be approximately equivalent to that of the individual coal samples. More specifically, during the initial stage of the repeated immersion tests (0–3 cycles), there was a noticeable small-scale increase in water absorption. In the middle stage of the repeated immersion (3–6 cycles), the water content of the composite sample increased steadily. As the repeated immersion test progressed to the later stage (6–10 cycles), the moisture content of the composite sample exhibited rapid growth, which gradually slowed down until reaching a state of saturation. This indicates that as the number of repeated immersion tests increases, the internal microscopic original defects within the sandstone and coal samples undergo further development, connection, and expansion.

Consequently, the load-bearing structure of the roof–coal pillar experiences a pronounced short-slab effect, and the degradation of the coal pillar poses a significant threat to the safety of the entire underground reservoirs.

B. Evolution characteristics of mechanical properties

1. Mechanical strength characteristics

Figure 4(a) reveals that the stress–strain curves of the composite samples are affected by varying repeated immersion numbers, exhibiting similar change trends. The entire loading process can be divided into four stages: the crack closure stage, linear elastic stage, crack development stage, and post-peak stage. The increase in the cycle number causes the fracture closure stage to expand, resulting in an overall increase in sample porosity. The linear growth stage decreases with the cycle number. Consequently, the sample's elastic strain capacity deteriorates, and a significant range of plastic deformation occurs. The crack development stage exhibits fluctuations, which can be attributed to the characteristics of crack initiation, development, and expansion in the sample. The effect of repeated immersion complicates the crack development process of the composite samples. The post-peak stage exhibited various stress drop phenomena, and an increase in the cycle number led to evident evolutionary characteristics transitioning from brittle failure to ductile failure.

The stress threshold serves as an indicator of the internal structural changes of the composite samples during different loading stages. More specifically, the crack closure stress threshold reflects the initial crack density and geometry within the samples, while the crack initiation stress threshold signifies the initiation of new cracks in the samples. The crack initiation stress threshold indicates the stress level necessary for the initiation of new cracks. The crack damage stress threshold represents the initial stress during the stage of unstable crack propagation, while the peak strength corresponds to the final failure strength of the samples. According to Fig. 4(b), the repeated immersion behavior has a significant impact on each stress threshold of the composite samples, and each stress threshold shows a downward trend with the cycle number increasing, but the crack damage stress threshold shows different nonlinear change characteristics. As the cycle number of repeated immersion increased from 0 to 10, the stress thresholds for crack closure, crack initiation, crack damage, and peak strength decreased from 3.26 to 1.47 MPa, 5.72 to 2.59 MPa, 10.77 to 4.03 MPa, and 12.85 to 6.24 MPa, respectively. Compared with other stress threshold parameters, the decrease in the crack closure stress threshold is relatively mild, indicating that the repeated immersion effect caused varying degrees of slight initial damage to the samples. These initial damages continue to intensify during the loading of the samples, leading to the formation of weakened areas within the internal structure. This subsequently triggers the development, connection, and expansion of new cracks, resulting in nonlinear damage of varying degrees and scales within the composite sample. Furthermore, the damage characteristics associated with each stress threshold exhibit a pattern of slow deterioration followed by accelerated damage, which correlates with the observed trend of water content change in the composite samples.

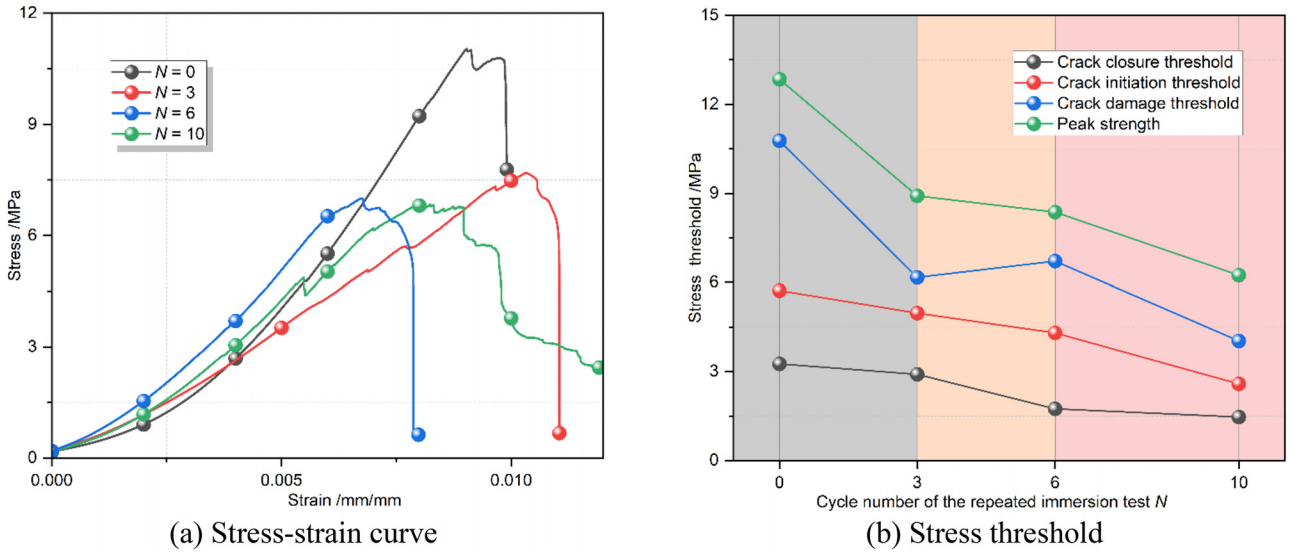

FIG. 4. Mechanical characteristics of composite samples.

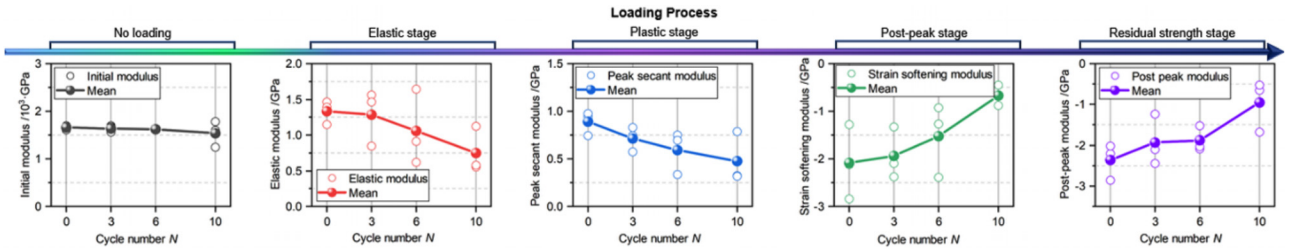

FIG. 5. Modulus parameters of composite samples at different loading stages.

2. Deformation resistance capability

As heterogeneous materials, natural rocks such as sandstone and coal exhibit strong anisotropy.[5] When studying these heterogeneous rocks, common methods for calculating the elastic modulus include the tangent line method, the secant line method, and the average modulus calculation method.[19,38] As depicted in Fig. 5, the variation in rock modulus parameters at different loading stages is dependent on the rock deformation capability. The initial modulus reflects the stress threshold required for the deformation and failure of the rocks without load. The elastic modulus indicates the rock's deformation resistance capability during the elastic stage of the loading process. The peak secant modulus represents the rock's deformation resistance capability in the elastic–plastic stage before reaching the peak. The softening modulus and post-peak modulus reflect the post-peak failure and residual deformation characteristics of the rocks, respectively.

It is evident that the various modulus values of the samples exhibit varying degrees of decrease trends under the influence of repeated immersion. This indicates that the samples have undergone the degradation effect caused by water. According to the loading stage of the samples, the initial modulus does not weaken significantly under the repeated immersion effect. The initial damage induced by the repeated immersion effect on the internal structure of the samples is not very significant. As the loading stage progressed to the linear elastic stage, the elastic modulus of the samples exhibited a significant decrease after six and ten times of repeated immersion, with reductions of 20.75% and 43.7%, respectively. This implies that the initial damage caused by the repeated immersion effect promotes the reduction of the friction coefficient between micro-cracks within the composite sample. The reduced relative sliding difficulty between the cracks leads to a significant decrease in the elastic modulus. This mechanical–hydro coupling effect accelerates the rapid degradation of the original defects in the composite samples.

Similar to the elastic modulus, the peak secant modulus represents the secant slope of the peak strength in the complete stress–strain curve, providing insights into the deformation characteristics of the pre-peak stage. As the cycle number of repeated immersion tests increased, the peak secant modulus exhibited a rapid decline trend, decreasing from the initial state of 0.889 to 0.716, 0.593, and 0.476 GPa, respectively. This indicates that the plastic deformation of the composite samples during the crack development stage significantly increased and became more complex under the degradation influence of the repeated immersion tests. In the post-peak failure stage and residual deformation stage of rocks, the strain softening modulus and post-peak modulus respectively characterize the strain softening behavior and residual deformation capacity of the rocks. Considering that the dam of the underground reservoir in coal mines is a rock mass subjected to frequent disturbances from overburden and *in situ* stress,[4] it is crucial to investigate the evolution characteristics of its strain softening modulus and post-peak modulus under the repeated immersion influence. The test results reveal a significant decline in both the strain softening modulus and post-peak modulus of the composite samples. After reaching its peak strength, the composite sample transitions into the post-peak stage, where post-peak failure characteristics become apparent. It rapidly unloads within a short period, exhibiting failure behavior. As the cycle number of repeated immersion tests increases, the degree of brittle failure in the composite samples diminishes, and a trend from brittle failure to ductile failure in the post-peak stage becomes evident. Therefore, the influence of mechanical loading on the post-peak stage of the samples starts to diminish, and the primary factor is the cumulative effect of degradation of the samples during the pre-peak loading process under repeated immersion effect.

To further investigate the impact of repeated immersion tests on the degradation of sandstone–coal composite samples, the stiffness evolution was analyzed, as depicted in Fig. 6. Stiffness refers to the amount of external force needed to induce a unit deformation in an

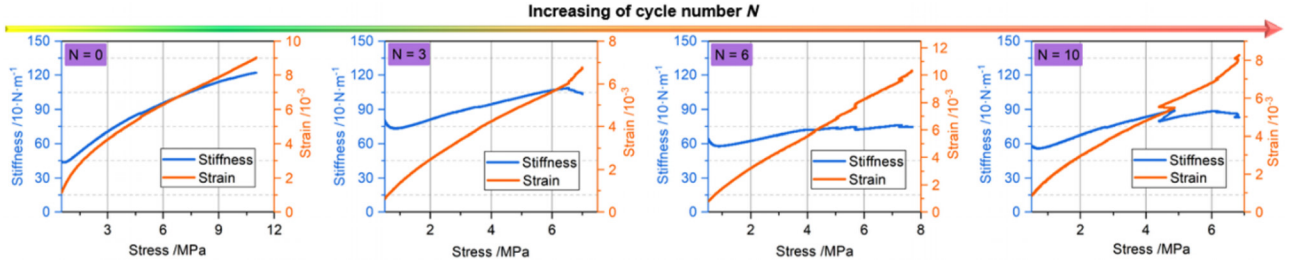

FIG. 6. Stiffness of composite samples.

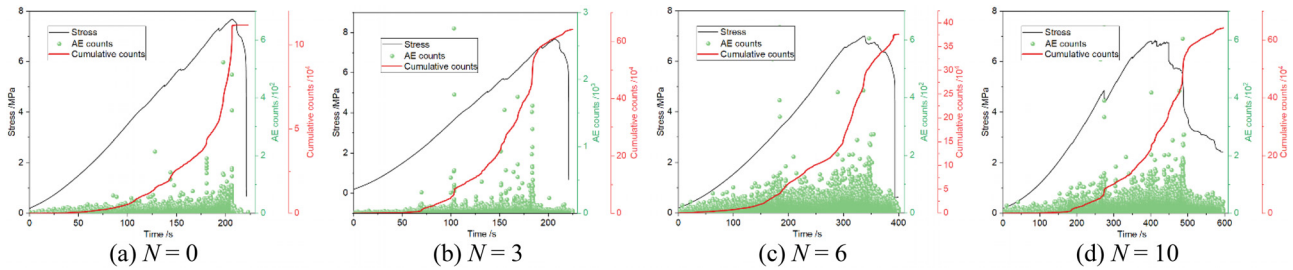

FIG. 7. AE counts of composite samples.

object.[19,38] The increase in the cycle number of repeated immersion tests leads to a gradual decrease in the slope of the stiffness curve. Stiffness transitions from a steady increase during the initial elastic stage to a slower increase or even a fluctuating softening trend during the plastic stage.

The intersection point of the stiffness–stress curve and the strain–stress curve corresponds to the unstable crack development stage of the composite samples. When the cycle number of repeated immersion tests reaches three times, the stiffness of the samples initiates a decline and fluctuations at the intersection point. The stress range corresponding to the intersection point is continuously decreasing, which also shows that the elastic stage of the samples is continuously reduced under the influence of repeated immersion tests. The plastic deformation of the samples is becoming more and more intense, which shows significant deterioration characteristics.

C. Acoustic emission characteristics

1. AE temporal domain and frequency domain parameters

The distribution density of acoustic emission (AE) counts serves as an indicator of the acoustic signal's intensity released during the initiation and propagation of internal defects within the composite sample. Through the analysis of the evolutionary characteristics of AE counts subjected to cyclic water immersion, insights into the degradation patterns of the composite sample under load can be gleaned, as depicted in Fig. 7. Initially, when $N = 0$, indicating no water-induced degradation, the AE count signals are concentrated in proximity to the peak stress. As the number of cycles progresses from 0 to 3, 6, and 10, correspondingly, the distribution range, density, and intensity of AE counts progressively escalate. This observation suggests that repetitive water immersion leads to incremental damage to the composite sample, resulting in a gradual weakening of its mechanical properties.

Furthermore, the cumulative AE counts provide a measure of the overall damage sustained by the composite sample throughout the loading process. With an increase in the number of cyclic water immersions, the inflection point of the cumulative AE counts curve shifts forward from the vicinity of the peak stress point to the plastic deformation stage. This shift signifies the outward manifestation of the acoustic emission signal, reflecting the continuous deterioration of the internal structure of the composite sample due to cyclic water immersion.

As illustrated in Fig. 8, when there is no water immersion (0 times), the AE energy distribution is minimal near the sample's crack closure stress threshold. However, once the loading load reaches the crack initiation stress threshold, the release of AE energy from the samples becomes more active. AE energy primarily concentrates around the crack damage stress threshold and the peak strength threshold. This is because during the initial loading stage of the samples, the cracks primarily undergo compaction effects, and no noticeable damage occurs. Once the sample is loaded to the crack damage stress threshold point, it transitions into the plastic deformation stage. Its internal micro-defects begin to exhibit more severe damage. As the cycle number increases, the intensity of the AE energy release gradually diminishes. It is only when the cycle number of repeated immersion tests reaches ten times that the sample incurs huge damage during the loading process, resulting in an evident local release of high-intensity AE energy. As the sample's elastic stage progressively diminishes, the plastic deformation characteristics become increasingly pronounced. The elastic energy is consistently transformed into plastic energy, resulting in a continuous reduction in both the distribution range and intensity of the AE energy. With an increasing number of cyclic water immersions, the inflection point of the cumulative AE energy curve

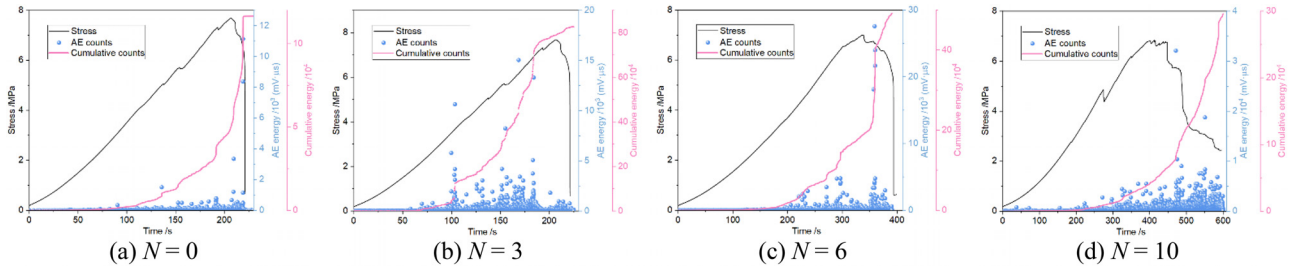

FIG. 8. AE energy of composite samples.

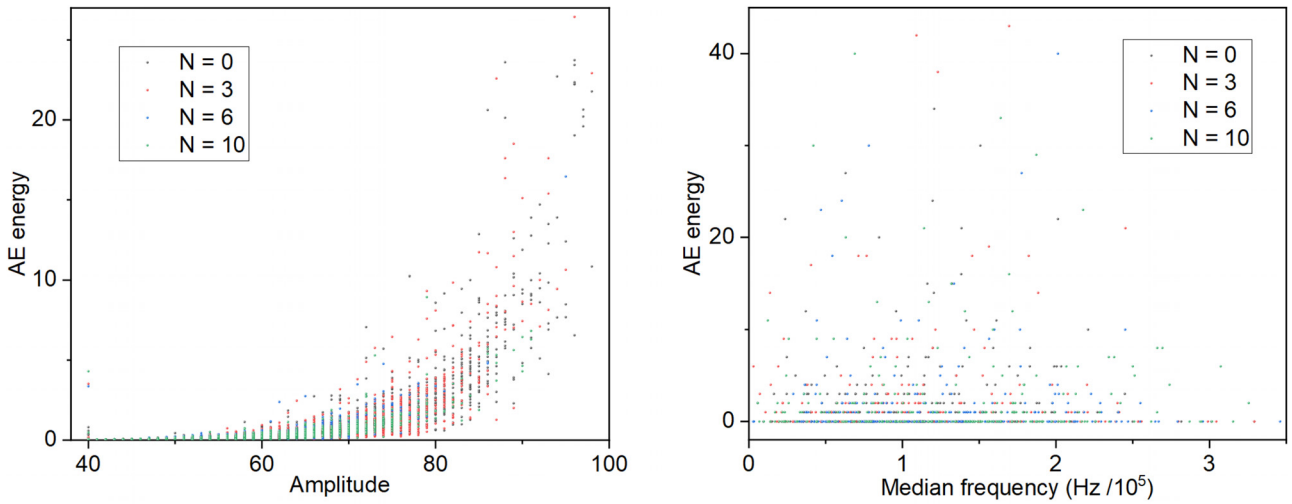

(a) Plots of AE energy versus amplitude (b) Plots of AE energy versus median frequency

FIG. 9. AE frequency domain parameters.

shifts forward from the vicinity of the peak stress point. The cyclic water immersion effect prompts a heightened release frequency of the AE energy signal during the plastic deformation stage of the composite sample, leading to an augmented degree of deterioration in the composite material.

Based on the analysis of AE temporal domain characteristics, we can further examine the degradation impact of repeated immersion on sandstone–coal composite samples by considering AE frequency domain characteristics.[39–41] Among these, the plots of AE energy vs amplitude can reflect the intensity of crack activity at various scales, while the graphs of AE energy vs median frequency can illustrate the extent of energy release associated with crack expansion type and speed, as depicted in Fig. 9. Given significant overlap in the acoustic emission data from samples subjected to varying immersion times, this manuscript delves deeper into the refinement and analysis of AE frequency domain characteristics, as depicted in Figs. 10 and 11. Overall, these data enable quantitative characterization of the evolution of cracks and deformation failure characteristics of the composite samples under varying immersion times.

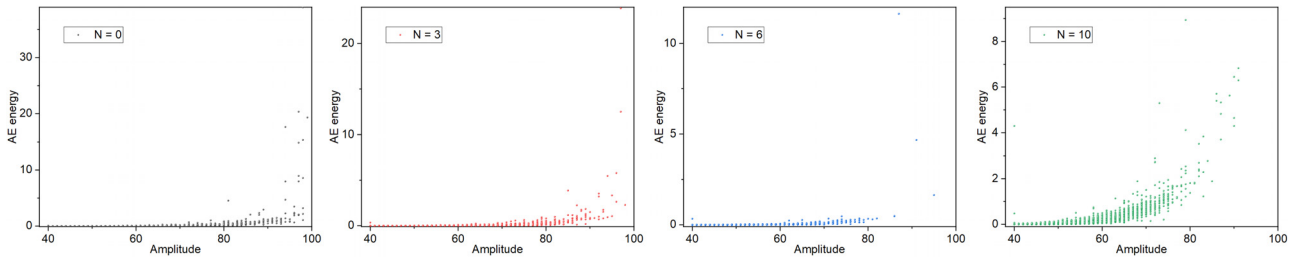

FIG. 10. Plots of AE energy vs amplitude under different repeated immersion cycles.

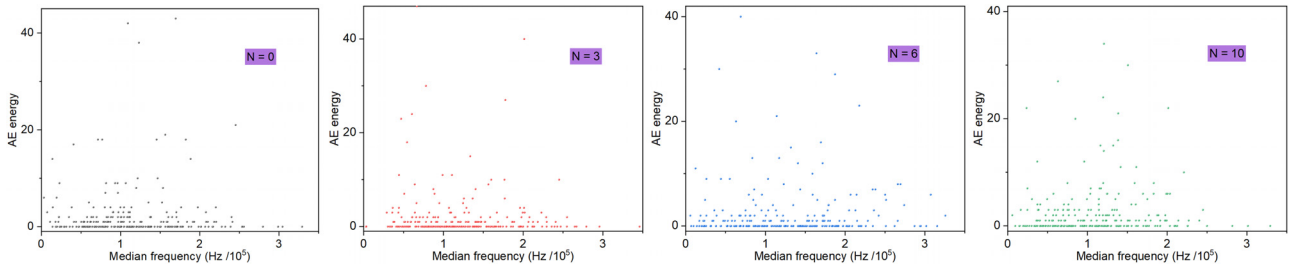

FIG. 11. AE energy of composite samples under different repeated immersion cycles.

As the number of repeated water immersions increases, the AE energy corresponding to the same amplitude gradually decreases. This indicates a reduction in the degree of acoustic emission energy release caused by crack expansion. However, the frequency of occurrence of acoustic emission signals has significantly increased, and their distribution range is further concentrated in the range of 40–95. This phenomenon further verifies that the composite samples deteriorated due to cyclic immersion. The samples underwent a more active microcrack initiation and development process under loading, leading to high-frequency acoustic emission energy release and significant sample damage.

Additionally, concerning the median frequency, the signal distribution range primarily falls between 0 and 380 kHz. Furthermore, most acoustic emission signals exhibit low amplitude and wide spectrum characteristics. Under the influence of cyclic water immersion, the acoustic emission signals are more broadly distributed in the low-frequency range. This indicates that cyclic water immersion accelerates the aging and damage of sandstone–coal composite samples. Under load, local stress rapidly concentrated within the composite sample that had undergone cyclic immersion. This led to the sample fracturing among its structural particles and generating a large number of microcracks shortly after loading. Consequently, the acoustic emission signal exhibited a significant surge in frequency. Specifically, the cyclic immersion effect concentrates the median frequency of acoustic emission of composite samples between 0 and 200 kHz. As the number of cyclic immersions increases from 0 to 10 times, the AE energy corresponding to the low median frequency gradually increases, and its distribution density also increases. This indicates that the expansion speed and scale of internal cracks in composite samples increase, and cyclic immersion accelerates the damage and aging of the internal structure of composite samples.

2. Real-time destruction scale analysis based on AE-b value

Acoustic emission mainly originates from the release of elastic energy when micro-defects within the rock undergo destruction.[29] This provides a valuable means to characterize the damage evolution process, including the initiation, development, and propagation of microcracks during the loading and failure of the samples.

Building upon this foundation, a comprehensive assessment of the influence of repeated water immersion on the failure precursor characteristics of the roof–coal pillar composite structure was conducted, utilizing the AE-b value, as depicted in Fig. 12. Generally, during the crack closure stress threshold and crack initiation stress threshold stages, the composite specimen exhibits no A-b value. These stages fall within the elastic range of the sample, indicating the absence of irreversible deformation. With an increase in axial load, the AE-b value signal emerges within the sample at the crack damage stress threshold stage, reaching a high value, signifying a relatively stable activity of AE events. As the stress loading transitions from the crack damage stress threshold to the peak stress, the A-b value exhibits a fluctuating downward trend.

Specifically, when $N = 0$, the AE-b value signal manifests at 270 s, reaching a peak level of 6.37, followed by a decline to the lowest value of 5.60 at 400 s. This initial significant decrease in the AE-b value during the loading process of the specimen indicates the generation of a substantial range and quantity of microcracks within the specimen, serving as a precursor signal for the composite specimen failure. Subsequently, the AE-b value experiences considerable fluctuations, corresponding to variations in AE energy. Ultimately, the specimen fails and undergoes complete destruction. For $N = 3$, the AE-b value signal first appears at 135 s (6.07) and drops to 5.60 at 203 s. This loading stage represents the precursor phase of specimen failure, accompanied by the generation and rapid expansion of numerous cracks within the specimen. The AE-b value undergoes a second decrease, reaching the minimum value of 5.16 at 219 s, culminating in the rapid and complete failure of the sample. In the case of $N = 6$, the AE-b value experiences a single decrease, transitioning from the maximum value of 6.58 at 207 s to the minimum value of 6.26 at 290 s. During this period, the sample has not yet undergone complete failure; the AE-b value increases with the load, and the sample sustains further damage until eventual failure. For $N = 10$, the AE-b value follows a similar trend, decreasing from the maximum value of 7.44 at 230 s to the minimum value of 6.43 at 349 s. However, it is noteworthy that the AE-b value exhibits a lower initial value (7.04) at 222 s, indicating more extensive damage to the sample and heightened susceptibility to large-scale damage.

3. Real-time crack generation type based on RA-AF parameters

In accordance with industry standards established by the Japan Association for Nondestructive Testing of Reinforced Concrete Structures, the correlation between AF-RA plays a crucial role in identifying the failure mode of cracks. Typically, tensile cracks demonstrate elevated AF/RA values, whereas shear cracks tend to display lower AF/RA values, as illustrated in Fig. 13. Therefore, the repeated immersion behavior's impact on the shear

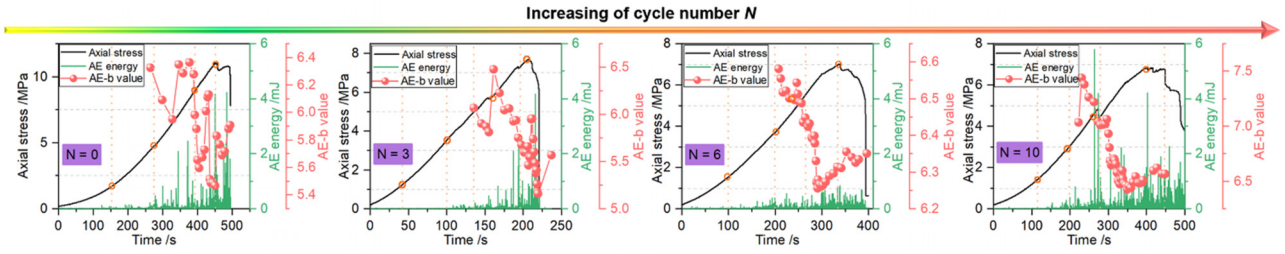

FIG. 12. AE-b value of composite samples.

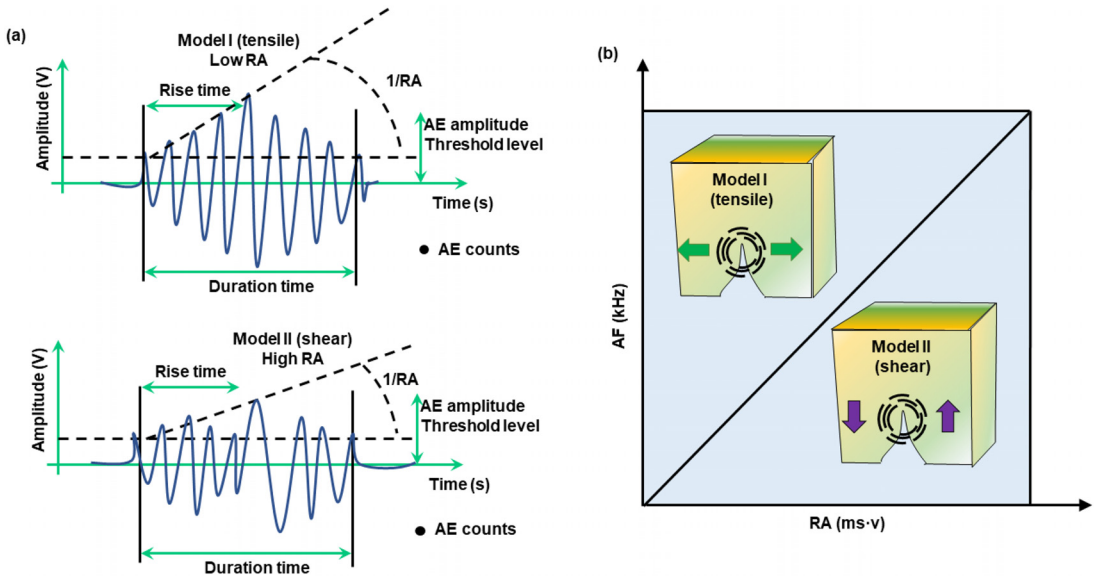

FIG. 13. Definition of RA-AF parameter and crack types. (a) Definition of RA-AF value. (b) Schematic of tensile/shear crack.

crack and tensile crack characteristics of the samples can be determined through the RA and AF parameters.[42,43]

As illustrated in Fig. 14, the crack evolution patterns of composite samples under varying immersion times exhibit a notable similarity. The majority of RA and AF signal values cluster near the coordinate axis, highlighting the distinct initiation, development, and expansion of both type I and type II cracks during the loading process. The region of intensive signal distribution consistently aligns with the tensile crack characteristic area, underscoring that tensile cracks predominantly contribute to the sample's damage throughout the loading sequence. With an increase in the number of repeated water immersions, the signal core distribution area, highly concentrated near the AF axis, gradually shifts toward the distribution proximity of the RA axis. This shift indicates a discernible trend in the increased proportion of shear cracks in activities such as crack initiation, development, and expansion within the composite sample. Consequently, the degree of deterioration in the composite sample expands, concurrently enhancing the anisotropic characteristics of its internal structure. Upon reaching a cycle number of 10, both tensile and shear cracks in the sample experience a significant escalation. This phenomenon is ascribed to the recurring immersion effect, which undermines the initially stable internal structure of the composite samples, inducing nonlinear damage. With an escalating cycle number, the sample undergoes progressive degradation, manifesting an increasing inclination toward compound cracks. Furthermore, disparities emerge in the crack evolution patterns of composite samples. As the number of repeated water immersions increases, the acoustic emission signal intensity gradually amplifies within the shear crack area. The principal distribution range of RA expands from 50 to 500 ms/V, accentuating the heightened activity of shear cracks in the composite sample.

To delve into the intricate details of crack evolution characteristics at each stage of the loading process, a thorough analysis of real-time changes in the curves corresponding to AE signals for both tensile and shear cracks was conducted. With the gradual increase in the number of repeated water immersions, the active period of the AE signal consistently advances. This progression signifies that repeated water immersion exacerbates internal defects in the composite sample, leading to a corresponding deterioration in its mechanical properties. As the specimen approaches failure, the cumulative number of tensile crack signals typically exceeds that of shear crack signals. Although repeated water immersion results in a gradual increase in the

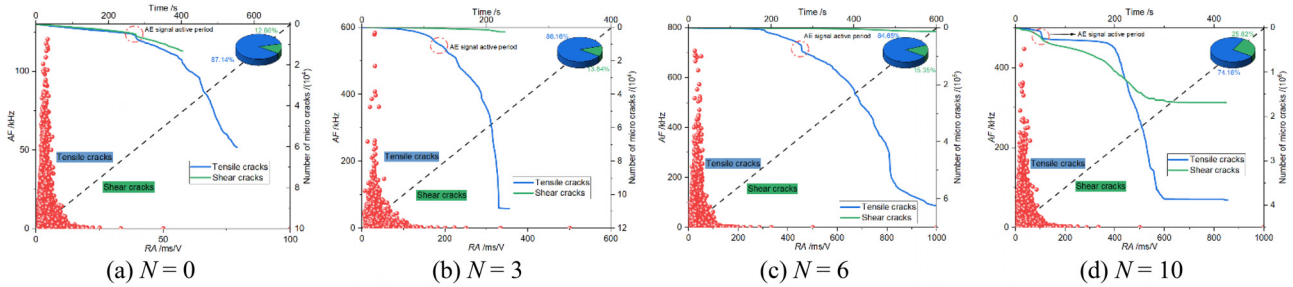

(a) $N = 0$ (b) $N = 3$ (c) $N = 6$ (d) $N = 10$

FIG. 14. Cracks initiation evolution characteristics of composite samples with different immersion times.

cumulative number of shear crack signals, it remains lower than the number of tensile cracks. This shift indicates that repeated water immersion intensifies shear damage in the composite sample, with a substantial number of shear cracks gradually becoming the primary contributing factor to failure under high loads. Moreover, the proportion of tensile cracks to shear cracks follows a similar evolving trend. As N increases from 0 to 10, the proportion of shear cracks rises from 12.86% to 25.82%, signifying a significant proliferation of shear cracks. This trend aligns with the aforementioned research findings, highlighting that repeated water immersion alters the crack evolution mechanism of the composite sample and expedites its fracture process.

D. Strain energy evolution

The loading process of rock involves energy input and dissipation.[29,44,45] By analyzing the energy evolution characteristics of composite samples under the repeated immersion effect, we can more comprehensively reveal their damage characteristics. Assuming no heat exchange between the rock and the external environment, the loading process entirely converts the mechanical energy into strain energy stored by the rock and energy dissipated through surface wear, radiation, and frictional heat. The process of energy evolution in rock encompasses the input energy (U), the elastic strain energy (U_e), the dissipated energy (U_d), and the post-peak released energy (U_r). Hence, the theoretical energy evolution process during rock loading under the repeated immersion effect is depicted in Fig. 15.

The strain energy relationship of composite samples under uniaxial compression tests is as follows:[45]

$$U = \int_0^{\varepsilon} \frac{\sigma_i + \sigma_{i+1}}{2} d\varepsilon = U_d + U_e, \tag{1}$$

where σ_i and σ_{i+1} represent the stress on the left and right of the microelement trapezoid, respectively, while ε denotes the strain experienced by the sample when it reaches peak strength,

$$U = \int_0^{\varepsilon_1} \sigma_1 d\varepsilon_1 + \int_0^{\varepsilon_2} \sigma_2 d\varepsilon_2 + \int_0^{\varepsilon_3} \sigma_3 d\varepsilon_3, \tag{2}$$

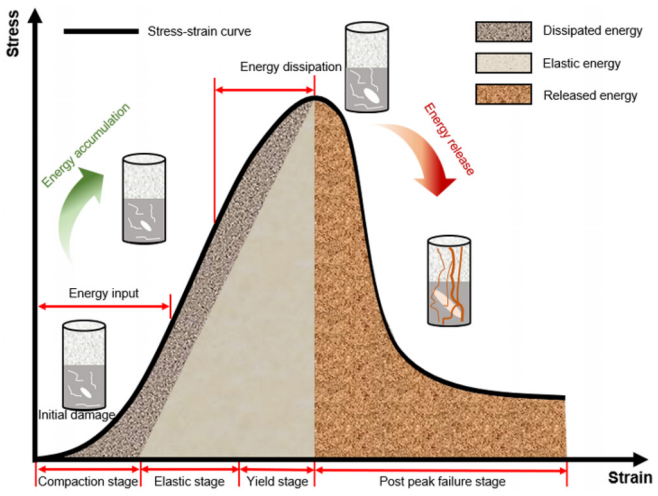

FIG. 15. Energy evolution characteristics of rocks under uniaxial compression.

$$U_e = \frac{1}{2\bar{E}}\left[{\sigma_1}^2 + {\sigma_2}^2 + {\sigma_3}^2 - 2\nu(\sigma_1\sigma_2 + \sigma_2\sigma_3 + \sigma_1\sigma_3)\right], \tag{3}$$

where U, U_e, and U_d represent the input strain energy, elastic strain energy, and dissipated strain energy, respectively. The variables σ_1, σ_2, and σ_3 denote the external stress applied to the material in three directions, while ε_1, ε_2, and ε_3 represent the corresponding strains resulting from stress application. E and ν are the material's elastic modulus and Poisson's ratio, respectively. Notably, since no confinement exists in the uniaxial compression test, implying $\sigma_2 = \sigma_3 = 0$, we can simplify Eqs. (2) and (3) to the following forms:[45]

$$U = \int_0^{\varepsilon_1} \sigma_1 d\varepsilon_1, \tag{4}$$

$$U_e = \frac{\varepsilon_e \sigma_1}{2}, \tag{5}$$

$$U_d = U - U_e = \int_0^{\varepsilon} \frac{\sigma_i + \sigma_{i+1}}{2} d\varepsilon - \frac{\varepsilon_e \sigma_1}{2}. \tag{6}$$

U_r signifies the total energy released from the peak strength stage to the residual deformation stage, as represented in Eq. (7). If there are no post-peak characteristics in the stress–strain curve, the released energy is roughly equivalent to the elastic strain energy prior to the peak,[29,45]

$$U_r = \int_{\varepsilon_e}^{\varepsilon_c} \frac{\sigma_i + \sigma_{i+1}}{2} d\varepsilon. \tag{7}$$

As demonstrated in Fig. 16, with an increase in the cycle number of repeated immersion tests, the input energy required for the failure of the composite sample progressively decreases, alongside a gradual reduction in its strain range. This suggests that the repeated immersion effect impairs the composite sample's capacity to accumulate strain energy, resulting in damage to the sample's internal structure. As the cycle number increases, both the elastic strain energy and dissipated energy decrease gradually, accompanied by a consistent narrowing of their strain range. Until the cycle number reaches 10, the proportion of stored elastic energy in the sample's input energy continues to shrink. This trend weakens the sample's elastic properties, leading to a gradual transition toward plasticity. This demonstrates the pronounced softening effect of repeated immersion on the composite sample. As the cycle number increases, both the post-peak released energy of the composite sample and the slope of its corresponding curve diminish. This demonstrates a clear transition in the sample, under the influence of repeated immersion, from exhibiting brittle failure characteristics to ductile failure. Specifically, when the cycle number is 0, the sample's brittle failure characteristics are prominent; it rapidly fails and releases energy after the peak point. With the cycle number increasing to 3, the slope of the post-peak release energy curve diminishes, indicating the onset of ductile failure characteristics in the sample. However, at this stage, the sample retains much of its bearing capacity and shows only minor signs of deterioration. As the cycle number increases, the sample's ductile failure characteristics become increasingly pronounced, and the degree of internal deterioration escalates significantly. At this stage, the sample can no longer maintain its load-carrying capacity and loses its energy storage capabilities. Consequently, there is a rapid decrease in the sample's post-peak release energy.

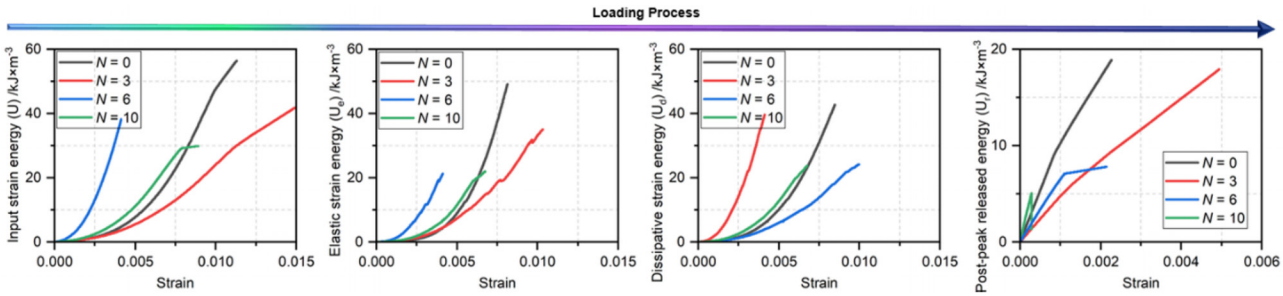

FIG. 16. Strain energy evolution of sandstone–coal composite samples.

IV. MECHANICAL DETERIORATION LAW OF SANDSTONE–COAL COMPOSITE SAMPLES UNDER REPEATED IMMERSION EFFECT

A. Damage variable model

The energy evolution characteristics of sandstone–coal composite samples under the repeated immersion effects in uniaxial loading provide a foundation for interpreting the progressive degradation of their mechanical properties through a damage constitutive model. In the context of damage variable definition, Sevostianov *et al.* and Barile *et al.* proposed a definition of the damage variable grounded in the AE count observed during the uniaxial compression of coal samples. This variable serves as

$$D_L = \left(1 - \frac{\sigma_c}{\sigma_p}\right)\frac{C_d}{C_0}. \tag{8}$$

The damage constitutive model is

$$\sigma = (1 - D)E\varepsilon = \left[1 - \left(1 - \frac{\sigma_c}{\sigma_p}\right)\frac{C_d}{C_0}\right]E\varepsilon, \tag{9}$$

where D denotes the damage variable as defined by Barile *et al.* The term σ_c represents the residual strength of rocks, while σ_p stands for its peak strength. C_d is the cumulative AE count, and C_0 signifies the cumulative AE count corresponding to the material's entire loading process.

Ma *et al.*[1] proposed a modified definition of the damage variable D, based on the changes observed in the dissipative energy of the rock–coal composite during uniaxial compression tests. This was expressed as

$$D_M = \left(1 - \frac{\sigma_c}{\sigma_p}\right)\frac{U^d}{U^{d\max}}\left(1 + \frac{U_d}{U}\right), \tag{10}$$

where U^d signifies the dissipative energy during the deformation and damage process of the rock, while U^{dmax} represents the cumulative dissipative energy necessary for complete rock failure. U_d is the dissipative energy at peak strength, and U is the total input energy at this peak strength level.

Ma *et al.*[1] posited that dissipative energy not only contributes to the rock's failure but also partially dissipates in various forms such as sound and heat, among others. Thus, the defined damage variable holds greater significance. Based on the dissipative energy characteristics, they modified a damage constitutive model for water-immersed rock under uniaxial compression tests. This model is

$$\sigma = (1 - D)E\varepsilon = \left[1 - \left(1 - \frac{\sigma_c}{\sigma_p}\right)\frac{U^d}{U^{d\max}}\left(1 + \frac{U_d}{U}\right)\right]E\varepsilon. \tag{11}$$

Since the repeated immersion effect is a dynamically changing damage effect, the above damage variable model cannot accurately describe the damage degree change of the sandstone–coal composite sample under the repeated immersion effect. Based on the effective stress theory, this paper introduces the concept of the softening coefficient's deterioration degree. This can serve as a reflection of the uniaxial mechanical strength degradation in composite samples under repeated immersion effects as follows:

$$\eta = \frac{\sigma_{sp}}{\sigma_{ip}}, \tag{12}$$

$$\sigma_I = \sigma_i'(1 - D) = \sigma_i'\left(1 - \frac{\sigma_{sp}}{\sigma_{ip}}\right), \tag{13}$$

where η is the softening coefficient of the uniaxial mechanical strength. σ_{sp} is the uniaxial compression strength of saturated composite samples under different cycle number of repeated immersion tests, and σ_{ip} is the uniaxial compression strength of dry composite samples. σ_I is the nominal stress, and σ_i is the effective stress.

Based on Eq. (11), considering the softening coefficient's deterioration degree, the damage variable D model is further refined as

$$D_J = \left(1 - \frac{\sigma_{sp}}{\sigma_{ip}}\right)\frac{U^d}{U^{d\max}}\left(1 + \frac{U_d}{U}\right). \tag{14}$$

Based on Eq. (14), the damage variable value for the composite samples was calculated using the softening coefficient and energy evolution characteristic parameters. As depicted in Fig. 17(a), we have assumed that the dry samples represent the original state.

With the cycle number increasing from 0 to 10 times, the strain range associated with the damage variable demonstrated a gradual decrease. Concurrently, the damage degree of the samples consistently escalated, resulting in damage variable values of 0.002, 0.302, 0.728, and 0.737. Notably, at the onset of the uniaxial loading test, the damage variable values for samples subjected to repeated immersion tests were uniformly low. This phase corresponds to the elastic stage of the composite samples, during which the internal original defects exhibit no substantial alterations. However, as the axial stress increases, the

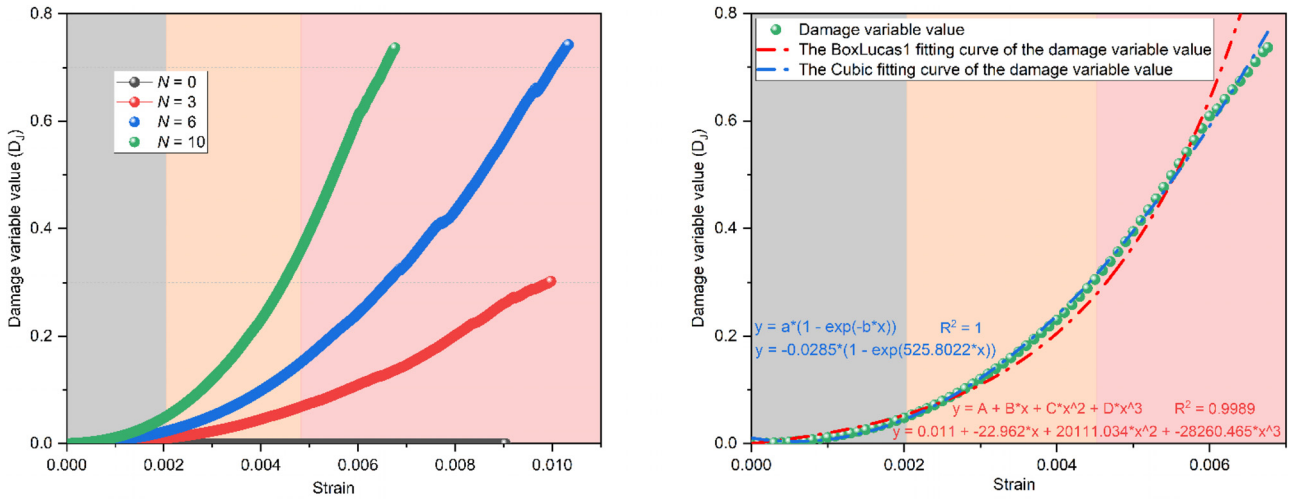

(a) Damage variable value of composite samples (b) Damage fitting curve under 10 cycle number

FIG. 17. Damage characteristics of composite samples under repeated immersion effect.

internal defects within the composite sample commence their expansion, precipitating the gradual formation of new cracks. Correspondingly, the damage variable value of the composite samples manifests a persistent increasing trend. With further increases in loading, the composite sample continually develops large-scale new cracks internally, leading to an accelerated growth rate of the damage variable. Upon failure of the composite sample, the damage variable experiences a rapid increase, resulting in the maximum damage degree of the samples. Moreover, considering a composite sample subjected to 10 cycle number of repeated immersion tests as an example, the fitting of the damage variable values demonstrates that the cubic nonlinear fitting curve model exhibits high precision, fully aligning with the test results, as illustrated in Fig. 17(b).

B. Damage constitutive model and the model verification

The moisture content serves as an indicator of the real-time alterations in the internal porosity of the composite sample, offering an indirect representation of the deteriorative impact of repeated water immersion on the sample's internal defects. Both dry strength and wet saturated strength provide indirect insights into the changes in the mechanical strength of the composite sample resulting from variations in moisture content. Consequently, drawing on the damage variable model mentioned above, a damage constitutive model for the composite sample under the influence of repeated immersion can be derived, contributing to the enhancement of its accuracy, as follows:

$$\sigma = (1-D)E\varepsilon = \left[1-\left(1-\frac{\sigma_{sp}}{\sigma_{ip}}\right)\frac{U^d}{U^{dmax}}\left(1+\frac{U_d}{U}\right)E\varepsilon\right]. \quad (15)$$

Theoretical stress–strain curves for the composite sample under repeated water immersion were calculated by considering the evolution characteristics of the damage variables. These theoretical curves were then compared with the corresponding experimental data, as illustrated in Fig. 18.

The theoretical stress–strain curve of the composite sample under repeated water immersion closely approximates the actual test values. This indicates that the theoretical model outlined in this manuscript effectively reproduces the pre-peak stress–strain changes in the composite sample, yet it struggles to accurately replicate the abrupt stress reduction observed in the post-peak stage. Furthermore, the mechanical strength calculated through theoretical derivation is marginally lower than the actual peak strength observed in experimental testing.

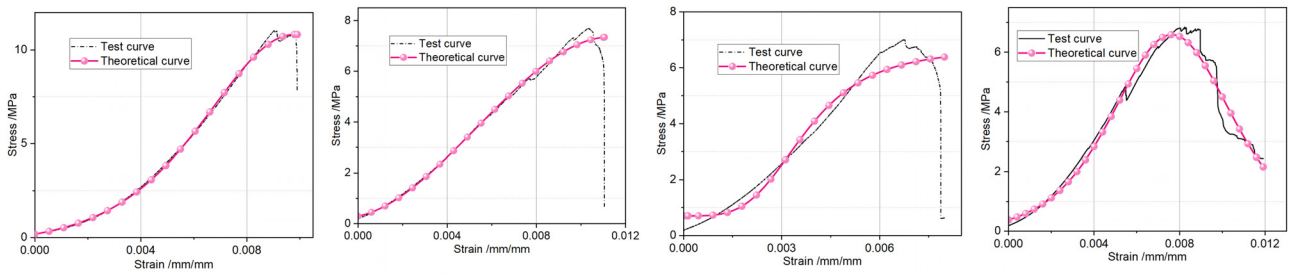

(a) $N = 0$ (b) $N = 3$ (c) $N = 6$ (d) $N = 10$

FIG. 18. Theoretical and experimental stress–strain curves of composite samples under repeated immersion effects.

This discrepancy highlights some limitations in measuring composite rock damage using strain energy and mechanical strength parameters after water immersion, underscoring the need for enhancements to the composite rock mass damage constitutive model. Nevertheless, with an increasing number of repeated immersions, the disparity between the theoretically derived curve and the actual curve gradually diminishes. This observation affirms that the improved constitutive model proves beneficial in analyzing the degradation process of mechanical properties in sandstone–coal composite samples subjected to prolonged repeated water immersion. It aids in discerning their long-term stability characteristics.

V. DISCUSSION

A. Differences in the effects of long-term immersion and repeated immersion

Long-term immersion behavior is a static mechanical–hydro coupling effect, which greatly differs from the actual engineering situation of the underground reservoirs in coal mines.[3] The "roof–coal pillar" bearing structure is exposed to a constantly changing moisture environment. Consequently, focusing solely on long-term immersion behaviors may not provide an adequate understanding of the damage and degradation characteristics of rock–coal composite seams under dynamic moisture environment changes. Based on the findings of previous studies,[35,36] this paper undertakes a comparative analysis of the composite samples under the long-term immersion effect and the repeated immersion effect. As depicted in Fig. 19, the water content, uniaxial compressive strength, and AE energy are compared using the normalization method.

1. Moisture content

Figure 19(a) displays the moisture content of the composite samples under both long-term immersion and repeated immersion, and the moisture content discrepancy escalated from 39% to 41%. The overall pattern of this moisture content difference demonstrated a trend of increase–decrease–substantial increase. In comparison to the 50-day period of long-term immersion test, frequent repeated immersion tests cause the original defects within the composite samples to deteriorate substantially, leading to a significant increase in moisture content.

2. Uniaxial compressive strength

Figure 19(b) depicts the normalized value of the sample's uniaxial compressive strength. The difference in uniaxial compressive strength remains relatively unchanged until the cycle number of repeated immersion is 6 and the duration of long-term immersion is 30 days. Based on the changes in moisture content, it can be inferred that the effective area of the composite samples diminishes. Consequently, the effective stress exerted on the sample intensifies, causing the samples to exhibit a decrease in uniaxial compressive strength. The deterioration of the uniaxial compressive strength of the composite samples under repeated immersion effect becomes more pronounced.

3. AE energy

As depicted in Fig. 19(c), the AE energy of the samples displays a downward trend as the duration of long-term immersion and the cycle number of repeated immersion tests increase. Notably, no significant difference is observed in the samples' AE energy when both the duration and the cycle number of immersion are relatively low. As two kinds of immersion tests progress, the AE energy under repeated immersion effects significantly decreases. Interestingly, repeated immersion effects, despite having a shorter effective immersion time, have caused a more pronounced degradation effect on the composite samples.

B. Meso-structure deterioration characteristics

From the perspective that macroscopic degradation of rocks under water–rock interaction is instigated by damage to their mesoscopic structure, this study investigates the deterioration characteristics of sandstone–coal composite samples under repeated immersion effects. The characteristics of the sandstone and coal are depicted in the SEM images shown in Fig. 20.

As the number of repeated immersion cycles increases, notable changes occur in the geometric properties of defects such as cementation degree, compactness of intergranular connections, pores, and

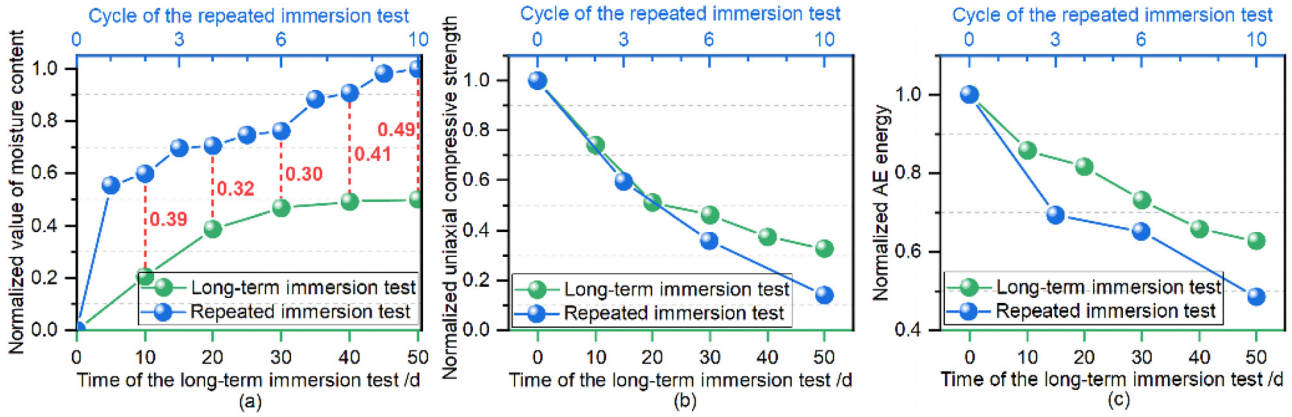

FIG. 19. Normalized parameter contrast of composite samples between the long-term and repeated immersion effects.

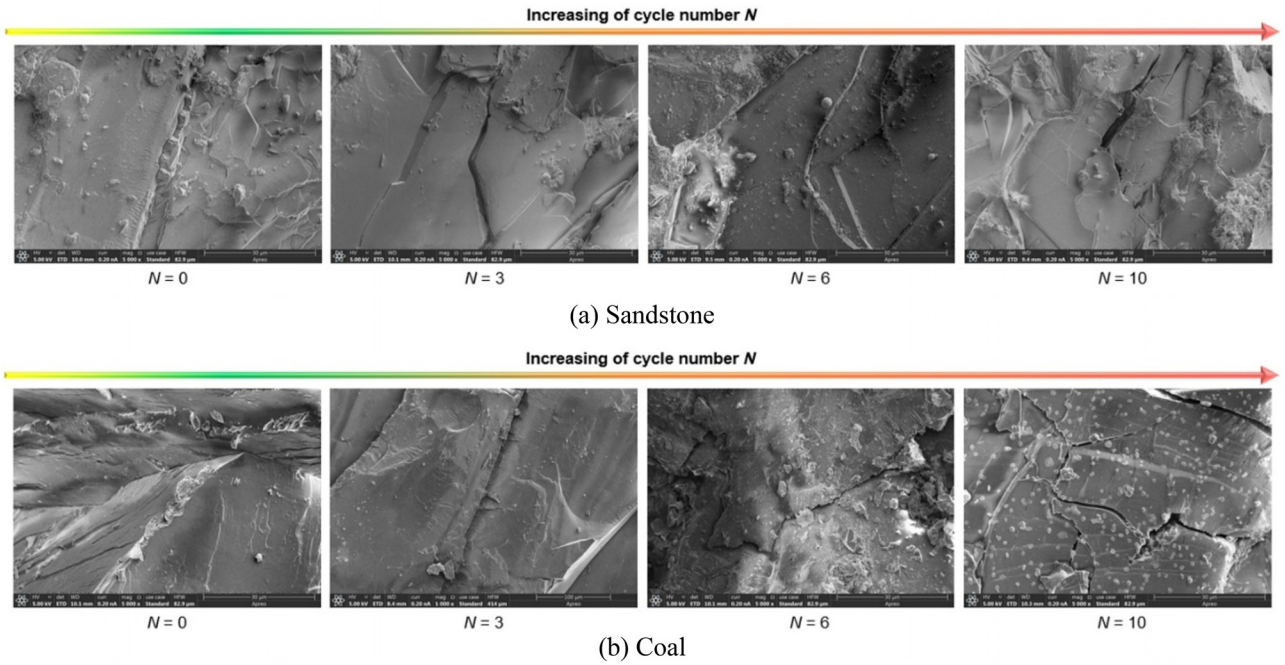

FIG. 20. Meso-structure of sandstone and coal.

cracks. Specifically, after 0 cycles of repeated immersion, the structures of sandstone and coal are relatively intact and dense. After 3 and 6 cycles of repeated immersion, both sandstone and coal begin to display signs of intergranular fracturing and bedding directional separation. Following 10 cycles, the structure of both sandstone and coal is noticeably fragmented, with larger broken particles appearing and a clear decrease in particle cementation density. Pores and cracks are prominently distributed throughout the structures of both sandstone and coal. Notably, the coal structure appears more fragmented than that of sandstone after 10 cycles of repeated immersion. This results in wider fissure openings, and the clay mineral particles within these fissures are expelled with each increased immersion cycle. Consequently, we can clearly observe clay mineral particles widely dispersed around the coal pores and fissures.

Water significantly weakens the cementing material between rock grains. The effect of repeated immersion alters the water content within the rock, leading to constant changes in the capillary pressure on its surface.[5] This initiates damage evolution in the sample, which progresses from the surface to the interior. Therefore, both sandstone and coal display a decrease in load bearing and deformation resistance capabilities at a macroscopic level.

C. Deterioration evolution mechanism of sandstone–coal composite samples under repeated immersion effect

Rock can be defined as an aggregate of particles or crystals cemented together.[5] The interaction effect between water and rock is a process wherein alterations in the microscopic structure result in changes to the macroscopic mechanical properties of the rock.[5] The principal factors influencing this water–rock interaction include the rock's mineral composition, microstructure, heterogeneity, the state of water flow, and temperature, among others.[5,14,37,38,46] The interaction between water and rock encompasses mechanical, physical, and chemical actions. Mechanically, this involves both hydrostatic and hydrodynamic pressure. Physically, it includes lubrication, softening, and mudification. Furthermore, from a microstructural and morphological standpoint, sandstone and coal harbor water-absorbing minerals.[5] These minerals, generate robust expansion pressure upon water absorption, and conversely, exhibit strong contraction pressure upon water loss.[5] For instance, the water-swelling pressure of clay minerals can reach a magnitude of 0.5–1.5 MPa.[45] This expansion pressure fosters the enlargement of original defects and the initiation of new cracks, which in turn damages the rock skeleton.[47]

Therefore, the repeated immersion behavior can exert both mechanical and physical effects on the rock, as depicted in Fig. 21. The dynamic fluctuation of water content induces a certain dynamic capillary pressure differential on the rock surface, intensifying the mechanical influence of water on the rock. This in turn can facilitate the expansion, contraction, dissolution, and precipitation phenomena of clay minerals within the rock, thereby amplifying the physical impact of water on the rock. Consequently, repeated immersion behavior exerts a more pronounced deteriorating effect on rocks compared to long-term immersion behaviors.

Assessing from the standpoint of macroscopic mechanical strength characteristics, the stress threshold, elastic modulus, and AE parameters of the composite samples exhibit a deterioration trend with the increase in repeated immersion times. These parameters correspond with the elastic stage, plastic stage, and post-peak failure stage in the rock loading process. The samples' elastic phase shrinks, and its

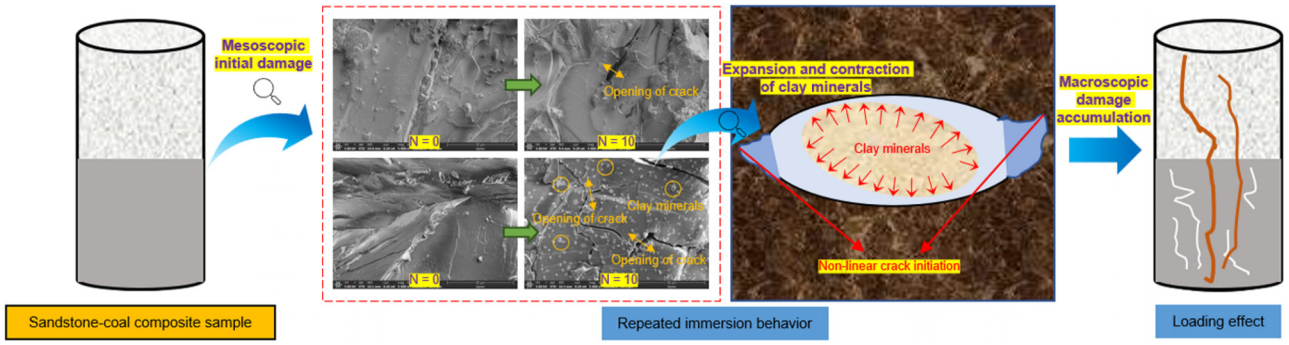

FIG. 21. Deterioration evolution mechanism of composite samples.

plastic phase expands. This shows that repeated immersion effect accelerates the rock plastic failure process, the rock plasticity is enhanced, and its failure characteristics have obvious brittle–ductile evolution phenomenon. The characteristics of the AE signal also show that the rock has obvious active crack formation after entering the plastic stage, and the formation of microcracks is mainly tensile cracks. However, after frequent deterioration by repeated immersion, there is an obvious increase in shear cracks. This also shows that the nonlinear change of rock is more complicated under the influence of repeated immersion.

Therefore, this mechanical–hydrological coupling effect constitutes a process wherein the water-induced erosion and damage of composite samples are continuously exacerbated by mechanical loading.

D. Implications for practical applications in underground reservoir management in coal mines

In the course of coal mining activities, disturbances to the surrounding rock formations are inevitable, resulting in the formation of water-conducting cracks and the generation of significant quantities of mine water. Traditionally, a substantial portion of this mine water is discharged onto the ground to facilitate safe and efficient production. However, this practice not only leads to the depletion of groundwater resources in the mining vicinity but also causes considerable damage to the surface ecology of the area, contributing to land salinization. Consequently, the reduction and prevention of mine water discharge onto the ground have emerged as critical technical challenges for the sustainable development of coal mining, representing a strategic objective for conserving and utilizing water resources within the coal mining sector.

As an innovative form of underground water management infrastructure, coal mine underground reservoirs are composed of goafs, safety coal pillars, artificial dams, and water intake facilities. Analogous to surface reservoirs, the safety and stability of the dam body are paramount for ensuring the safety of coal mine underground reservoirs. The dam body of an underground reservoir in a coal mine consists of coal pillars left behind during mining at the working face, along with an artificial dam. These residual coal pillars serve as the primary component of the dam, playing a crucial role in mitigating water damage, controlling ground pressure, minimizing surface losses, and ensuring roadway stability. Therefore, their presence is indispensable for overall dam stability and the sustained operation of water storage facilities.

While surface reservoir dams are subject to strict specifications during design and construction, with continuous safety monitoring and management measures during reservoir operation, they also undergo risk analyses to assess the impact of crack propagation on dam safety and stability. The natural and man-made earthquakes can cause significant damage to surface reservoir dams, necessitating comprehensive research into their effects on dam safety. In contrast, coal mine underground reservoir dams operate under more intricate conditions, being located underground and subject to the combined pressures of overlying rock-coal pillar composite structures, mine pressures, and water pressures. Consequently, earthquakes or mining-induced tremors can trigger water outbursts from the reservoir, posing risks to underground production safety. Hence, the investigation into crack propagation and failure modes of roof–coal pillar structures, as undertaken in this study, is essential for understanding the stability of coal pillar dams within coal mine underground reservoirs under unique operational conditions.

The enhanced constitutive model predicts the mechanical strength of sandstone–coal composite samples by dynamically measured damage parameters, enabling real-time prediction of the mechanical strength degradation characteristics of the composite structures. By continuously updating mechanical parameters in real-time, it facilitates the design of the length, width, and height dimensions of the roof–coal pillar composite structure under water–rock effects, while also enhancing the damage assessment method. By comparing the predicted mechanical parameters of composite samples with actual mechanical threshold parameters, it can guide backfill or grouting material selection for roof–coal pillar composite structures and assist in risk prediction and management.

VI. CONCLUSION

To study the characteristics and mechanisms underlying the mechanical strength deterioration in sandstone–coal composite samples subjected to repeated immersion effect, we conducted uniaxial compression tests on the composite samples with varying cycle number of repeated immersion. The main conclusions obtained are as follows:

(1) Due to repeated immersion effects, the deterioration degree of stress thresholds and modulus parameters of the composite

samples increases. Noticeable cumulative damage effects can be further induced by the loading process.

(2) The crack characteristics of the composite samples, as delineated by AE parameters, predominantly consist of tensile cracks. However, the frequency of shear cracks tends to incrementally increase with rising cycle numbers of repeated immersion tests. The initiation of microcracks within the composite samples progressively displays stronger nonlinear characteristics.

(3) The mesoscopic structure of the sandstone and coal undergoes continuous degradation under repeated immersion effects. Internal defects gradually expand, the opening of cracks significantly alters, and clay minerals exhibit evident dissolution and precipitation. This meso-structure deterioration results in the increase of water storage space, thereby exacerbating the composite sample degradation.

(4) The constitutive model of the composite sample was improved based on the degradation characteristics of mechanical strength and strain energy parameters following repeated water immersion. Verification indicates that this modified model offers enhanced accuracy in analyzing the degradation process caused by water immersion, thereby providing valuable insights for determining the long-term stability of sandstone–coal composite samples.

Furthermore, surface reservoir dams are subject to stringent design and construction protocols, whereas underground reservoir dams contend with more intricate conditions, rendering them susceptible to earthquakes and mining-induced vibrations. Future research endeavors should concentrate on delving deeper into the determination and prediction of the instability failure mode of roof-coal pillar structures, particularly considering the influence of time effects. Such efforts will serve to augment our comprehension of the dynamic stability of underground reservoirs across various operational scenarios.

ACKNOWLEDGMENTS

The research described in this paper was financially supported by the K. H. Renlunds stiftelse (No. 14022020), the China Scholarship Council, and JSPS KAKENHI (Grant Numbers JP21K14575 and JP22K05005).

AUTHOR DECLARATIONS

Conflict of Interest

The authors have no conflicts to disclose.

Author Contributions

Tianqi Jiang: Methodology (equal); Writing – original draft (equal); Writing – review & editing (equal). **Chun Zhu:** Funding acquisition (equal); Methodology (equal); Supervision (equal); Writing – review & editing (equal). **Yang Qiao:** Conceptualization (equal); Funding acquisition (equal); Supervision (equal); Writing – review & editing (equal). **Takashi Sasaoka:** Conceptualization (equal); Writing – review & editing (equal). **Hideki Shimada:** Methodology (equal); Writing – original draft (equal). **Akihiro Hamanaka:** Conceptualization (equal); Methodology (equal). **Wei Li:** Writing – review & editing (equal). **Bingbing Chen:** Supervision (equal); Writing – review & editing (equal).

DATA AVAILABILITY

The data that support the findings of this study are available from the corresponding author upon reasonable request.

REFERENCES

[1]Q. Ma, Y. L. Tan, X. S. Liu, Q. H. Gu, and X. B. Li, "Effect of coal thicknesses on energy evolution characteristics of roof rock-coal-floor rock sandwich composite structure and its damage constitutive model," Compos. Part B: Eng. **198**, 108086 (2020).

[2]Y. Liu, M. Ji, Y. Wang, G. Liu, P. Gu, and Q. Wang, "Fractal mechanical model of variable mass seepage in karst collapse column of mine," Phys. Fluids **36**, 022031 (2024).

[3]M. B. Chi, Q. S. Li, Z. G. Cao, J. Fang, B. Y. Wu, Y. Zhang, S. R. Wei, X. Q. Liu, and Y. M. Yang, "Evaluation of water resources carrying capacity in ecologically fragile mining areas under the influence of underground reservoirs in coal mines," J. Cleaner Prod. **379**, 134449 (2022).

[4]C. Zhang, F. T. Wang, and Q. S. Bai, "Underground space utilization of coalmines in China: A review of underground water reservoir construction," Tunnel. Underground Space Technol. **107**, 103657 (2021).

[5]C. Zhang, Q. S. Bai, P. H. Han, L. Wang, X. J. Wang, and F. T. Wang, "Strength weakening and its micromechanism in water–rock interaction: A short review in laboratory tests," Int. J. Coal Sci. Technol. **10**, 10 (2023).

[6]A. J. Park and P. J. Ortoleva, "WRIS.TEQ: Multi-mineralic water–rock interaction, mass-transfer and textural dynamics simulator," Comput. Geosci. **29**, 277 (2003).

[7]C. J. Tang, Q. L. Yao, Q. Xu, C. H. Shan, J. M. Xu, H. Han, and H. T. Guo, "Mechanical failure modes and fractal characteristics of coal samples under repeated drying–saturation conditions," Nat. Resour. Res. **30**, 4439 (2021).

[8]H. L. Liu, W. C. Zhu, Y. J. Yu, T. Xu, R. F. Li, and X. G. Liu, "Effect of water imbibition on uniaxial compression strength of sandstone," Int. J. Rock Mech. Min. Sci. **127**, 104200 (2020).

[9]Á. Rabat, R. Tomás, and M. Cano, "Assessing water-induced changes in tensile behaviour of porous limestones by means of uniaxial direct pull test and indirect methods," Eng. Geol. **313**, 106962 (2023).

[10]Y. Ding, D. Yin, H. Hu, Y. Tan, H. Liu, X. Li, and N. Jiang, "Influence characteristics and macro-meso mechanism of pressure immersion time on tensile properties for coal materials," J. Mater. Res. Technol. **26**, 2358 (2023).

[11]Y. Malecot, L. Zingg, M. Briffaut, and J. Baroth, "Influence of free water on concrete triaxial behavior: The effect of porosity," Cem. Concr. Res. **120**, 207 (2019).

[12]C. D. Liu, Y. Cheng, Y. Y. Jiao, G. H. Zhang, W. S. Zhang, G. Z. Ou, and F. Tan, "Experimental study on the effect of water on mechanical properties of swelling mudstone," Eng. Geol. **295**, 106448 (2021).

[13]L. N. Y. Wong, V. Maruvanchery, and G. Liu, "Water effects on rock strength and stiffness degradation," Acta Geotech. **11**, 713 (2016).

[14]X. J. Yang, J. M. Wang, C. Zhu, M. C. He, and Y. Gao, "Effect of wetting and drying cycles on microstructure of rock based on SEM," Environ. Earth Sci. **78**, 183 (2019).

[15]Q. M. Wang, Q. H. Hu, C. Larsen, C. Zhao, M. D. Sun, Y. X. Zhang, and T. Zhang, "Microfracture-pore structure characterization and water-rock interaction in three lithofacies of the Lower Eagle Ford Formation," Eng. Geol. **292**, 106276 (2021).

[16]Y. Chen, P. Cao, D. W. Mao, C. Z. Pu, and X. Fan, "Morphological analysis of sheared rock with water–rock interaction effect," Int. J. Rock Mech. Min. Sci. **70**, 264 (2014).

[17]Q. Huang, M. Li, Y. Huang, A. Zhang, X. Lian, Y. Yan, and X. Feng, "Effect of inorganic salts in coal seams on the sand-carrying capacity of hydroxypropyl guar foam-fracturing fluid: An experimental study," Phys. Fluids **35**, 093118 (2023).

[18]X. Wang, J. Pan, Q. Hou, G. Li, L. Liu, Z. Wang, and L. Zhang, "Anisotropy of fracture and permeability in high-rank coal analyzed using digital rock physics," Phys. Fluids **35**, 093603 (2023).

[19]Q. L. Yao, C. J. Tang, Z. Xia, X. L. Liu, L. Zhu, Z. H. Chong, and X. D. Hui, "Mechanisms of failure in coal samples from underground water reservoir," Eng. Geol. **267**, 105494 (2020).

[20]T. Wang and C. Z. Yan, "Investigating the influence of water on swelling deformation and mechanical behavior of mudstone considering water softening effect," Eng. Geol. **318**, 107102 (2023).
[21]B. L. Liu, H. Q. Yang, and S. Karekal, "Effect of water content on argillization of mudstone during the tunnelling process," Rock Mech. Rock Eng. **53**, 799 (2020).
[22]C. J. Tang, Q. L. Yao, T. Chen, C. H. Shan, and J. Li, "Effects of water content on mechanical failure behaviors of coal samples," Geomech. Geophys. Geo-energy Geo-resour. **8**, 87 (2022).
[23]K. Wang, E. Zhao, Y. Guo, F. Du, and K. Ding, "Effect of loading rate on the mechanical and seepage characteristics of gas-bearing coal–rock and its mechanical constitutive model," Phys. Fluids **36**, 026606 (2024).
[24]Y. Chu, M. Wang, Y. Wang, S. Song, H. Liu, K. Ouyang, and F. Liu, "Damage characteristics of pore and fracture structures of coal with liquid nitrogen freeze thaw," Phys. Fluids **35**, 127114 (2023).
[25]Y. Yang, S. Wei, S. Wang, M. Wang, W. Shen, X. Li, and J. Kang, "Study on the deterioration characteristics and mechanism of physical and mechanical properties of natural gypsum rock under freeze–thaw action," Phys. Fluids **35**, 106606 (2023).
[26]J. Zhao, Q. Liu, C. Jiang, Z. Shupeng, Z. Weilong, and M. Hailong, "Dynamic mechanism of rock mass sliding and identification of key blocks in multi-fracture rock mass," Geomech. Eng. **32**, 375 (2023).
[27]H. Q. Song, J. P. Zuo, H. Y. Liu, and S. H. Zuo, "The strength characteristics and progressive failure mechanism of soft rock-coal combination samples with consideration given to interface effects," Int. J. Rock Mech. Min. Sci. **138**, 104593 (2021).
[28]J. P. Zuo, Z. F. Wang, H. W. Zhou, J. L. Pei, and J. F. Liu, "Failure behavior of a rock-coal-rock combined body with a weak coal interlayer," Int. J. Min. Sci. Technol. **23**, 907 (2013).
[29]Q. Ma, Y. L. Tan, X. S. Liu, Z. H. Zhao, and D. Y. Fan, "Mechanical and energy characteristics of coal–rock composite sample with different height ratios: A numerical study based on particle flow code," Environ. Earth Sci. **80**, 309 (2021).
[30]D. W. Yin, S. J. Chen, Y. Ge, and R. Liu, "Mechanical properties of rock–coal bi-material samples with different lithologies under uniaxial loading," J. Mater. Res. Technol. **10**, 322 (2021).
[31]J. Wang, J. X. Fu, W. D. Song, and Y. F. Zhang, "Mechanical properties, damage evolution, and constitutive model of rock-encased backfill under uniaxial compression," Constr. Build. Mater. **285**, 122898 (2021).
[32]Z. H. Zhao, W. M. Wang, L. H. Wang, and C. Q. Dai, "Compression–shear strength criterion of coal–rock combination model considering interface effect," Tunnel. Underground Space Technol. **47**, 193 (2015).
[33]K. Fang and M. Fall, "Shear behaviour of rock–tailings backfill interface: effect of cementation, rock type, and rock surface roughness," Geotech. Geol. Eng. **39**, 1753 (2021).
[34]C. Q. Zhu, H. Y. Ma, P. T. Zhao, J. W. Yue, and B. B. Wang, "Strength characteristics of frozen coal–rock interface for rock crosscut coal uncovering," Energy Explor. Exploit. **40**, 460 (2021).
[35]G. B. Chen, J. W. Zhang, T. Li, S. J. Chen, G. H. Zhang, P. F. Lv, and P. C. Teng, "Timeliness of damage and deterioration of mechanical properties of coal-rock combined body under water-rock interaction," J. China Coal Soc. **46**, 701 (2021), see http://mtxb.com.cn/en/article/id/44c94060-f9c7-4c04-bcb7-cb767bd1847f.
[36]G. B. Chen, T. Li, L. Yang, G. H. Zhang, P. F. Lv, and P. C. Teng, "Mechanical properties and damage characteristics of coal-rock combined samples under water-rock interaction," Coal Sci. Technol. **51**, 37 (2023), see http://www.mtkxjs.com.cn/en/article/doi/10.13199/j.cnki.cst.2020-1385.
[37]S. J. Chen, T. Q. Jiang, H. Y. Wang, F. Feng, D. W. Yin, and X. S. Li, "Influence of cyclic wetting-drying on the mechanical strength characteristics of coal samples: A laboratory-scale study," Energy Sci. Eng. **7**, 3020 (2019).
[38]Q. L. Yao, T. Chen, C. J. Tang, M. Sedighi, S. W. Wang, and Q. X. Huang, "Influence of moisture on crack propagation in coal and its failure modes," Eng. Geol. **258**, 105156 (2019).
[39]A. Vinogradov, A. Lazarev, M. Linderov, A. Weidner, and H. Biermann, "Kinetics of deformation processes in high-alloyed cast transformation-induced plasticity/twinning-induced plasticity steels determined by acoustic emission and scanning electron microscopy: Influence of austenite stability on deformation mechanisms," Acta Mater. **61**, 2434 (2013).
[40]E. Pomponi and A. Vinogradov, "A real-time approach to acoustic emission clustering," Mech. Syst. Signal Process. **40**, 791 (2013).
[41]A. Vinogradov, D. Orlov, A. Danyuk, and Y. Estrin, "Effect of grain size on the mechanisms of plastic deformation in wrought Mg–Zn–Zr alloy revealed by acoustic emission measurements," Acta Mater. **61**, 2044 (2013).
[42]Q. Zheng, Y. Xu, H. Hu, J. Qian, Y. Ma, and X. Gao, "Quantitative damage, fracture mechanism and velocity structure tomography of sandstone under uniaxial load based on acoustic emission monitoring technology," Constr. Build. Mater. **272**, 121911 (2021).
[43]Z. Xia, Q. Yao, X. Li, L. Yu, C. Shan, Y. Li, and Y. Hao, "Acoustic emission characteristics and energy mechanism of CFRP-jacketed coal specimens under uniaxial compression," Constr. Build. Mater. **342**, 127936 (2022).
[44]H. F. Ma, Y. Q. Song, J. K. Yang, J. J. Zheng, F. X. Shen, Z. X. Shao, and Z. G. Xia, "Experimental investigation on physical–mechanical behaviors and macro–micro-structural responses of lignite subjected to freeze–thaw cycles," Nat. Resour. Res. **32**, 543 (2023).
[45]H. F. Ma, Y. Q. Song, S. J. Chen, D. W. Yin, J. J. Zheng, F. X. Shen, X. S. Li, and Q. Ma, "Experimental investigation on the mechanical behavior and damage evolution mechanism of water-immersed gypsum rock," Rock Mech. Rock Eng. **54**, 4929 (2021).
[46]C. T. Johnston, *Clay Mineral–Water Interactions* (Elsevier, 2018).
[47]Q. J. Zhou, R. G. Deng, X. Wang, and K. Wang, "Experimental study on time-dependent deformation of red-bed mudstone," IOP Conf. Ser.: Earth Environ. Sci. **668**, 012065 (2021).